

Turn-On Circularly Polarized Luminescence in Metal–Organic Frameworks

Xue-Zhi Wang, Meng-Ying Sun, Zhijin Huang, Mo Xie, Ruishan Huang, Huihui Lu, Zujin Zhao, Xiao-Ping Zhou,* and Dan Li*

The fabrication of circularly polarized luminescence (CPL) active materials by self-assembly is still in its challenge. In this work, a family of homochiral metal–organic frameworks (MOFs) and metal–organic cages (MOCs) are constructed by solvothermal subcomponent self-assembly. These MOFs feature an eta topology with trifold helical chains, while the MOCs adopt a cubic cage structure. The chiral ligands show two distinct types of conformations: “opened” and “closed” in MOFs and MOCs, respectively. Although homochiral MOFs and MOCs show similar spectra of circular dichroism and photoluminescence with similar quantum yields and lifetimes, the MOFs yield clear CPL signals and the CPL of MOCs are silent. The turn-on CPL in MOFs achieved by tuning the conformation of ligands and controlling self-assembly provides a new approach for development of CPL-active MOF materials.

structures and advanced functions.^[6–8] MOFs can be endowed with homochiral property by incorporating with chiral ligands or supramolecular chirality around metal centers, which can be applied as potential materials for asymmetric catalysis^[9] and enantioselective recognition.^[10] However, the application of chiral MOFs as CPL-active materials has not been extensively studied yet and limited examples have been reported. Duan et al. reported the first example of CPL-active zeolitic imidazolate frameworks by a ligand-exchange approach in 2019.^[11] Thereafter, Zhang et al. synthesized new chiral MOF thin films exhibiting CPL property.^[12] Recently, Liu et al.

1. Introduction

Circularly polarized luminescence (CPL) materials, emitting the differential left- and right-handed circularly polarized light, have attracted great interest in recent years due to their promising applications in chemical sensors,^[1,2] biological probes,^[3] 3D display,^[4] and optical data storage.^[5] Various materials including organic molecules, polymers, metal–organic complexes, and liquid crystals have shown CPL-active properties. MOFs representing an interesting type of porous crystalline materials have been widely studied for their novel

have employed the aggregation-induced emission (AIE) ligand for the construction of CPL-active MOFs.^[13] Moreover, several CPL-active MOF materials have been achieved by using host–guest approach.^[14–18] For example, Liu et al. found that the chiral γ CD-MOF can emit CPL with the full-colored region after accommodating guest luminophores, such as dye molecules, AIE molecules, and Ru-complexes.^[19] To improve the CPL response, one important strategy adopted for organic systems is through the controlling self-assembly of chromophores.^[20,21] However, this strategy has not well been applied in the study of CPL-active MOF materials.

Herein, we report three enantiomeric pairs of MOFs with eta topology and cubic MOCs (metal–organic cages), which were obtained by solvothermal subcomponent self-assembly of 4-formylimidazole or its derivatives, chiral 1,2-diaminocyclohexane (DCH), and ZnBr₂ (Scheme 1). The change of the substituent of imidazole ligand on 2-position leads to yield distinct assemblies, in which the ligands adopt the “opened” (MOFs) or “closed” (MOCs) conformations. All enantiopure MOFs and MOCs showed strong circular dichroism (CD) signals and photoluminescence (PL) with similar quantum yields (QYs) and lifetimes in solid state. Surprisingly, only MOFs emit CPL. Density functional theory (DFT) calculations revealed that the possible mechanism is due to the efficient intramolecular charge transfer from the chiral cyclohexane moiety to the imidazolyl chromophore for “opened” conformation ligand in MOFs.


2. Results and Discussion

Previously, we found that the solvothermal subcomponent self-assembly is a convenient method to synthesize MOFs and

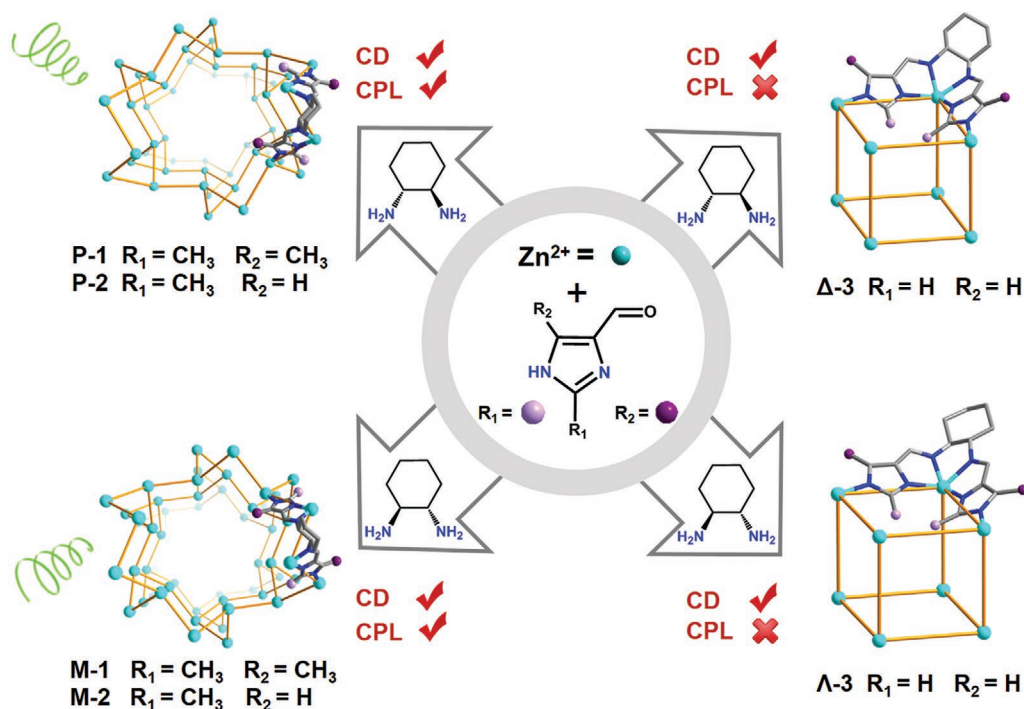
X.-Z. Wang, M.-Y. Sun, Dr. M. Xie, Prof. X.-P. Zhou, Prof. D. Li
College of Chemistry and Materials Science
Guangdong Provincial Key Laboratory of Functional Supramolecular
Coordination Materials and Applications
Jinan University
Guangzhou 510632, P. R. China
E-mail: zhoup@jnu.edu.cn; danli@jnu.edu.cn

Z. Huang, Prof. H. Lu
Guangdong Provincial Key Laboratory of Optical
Fiber Sensing and Communications
Department of Optoelectronic Engineering
Jinan University
Guangzhou 510632, P. R. China

R. Huang, Prof. Z. Zhao
State Key Laboratory of Luminescent Materials and Devices
Guangdong Provincial Key Laboratory of Luminescence
from Molecular Aggregates
South China University of Technology
Guangzhou 510632, P. R. China

 The ORCID identification number(s) for the author(s) of this article can be found under <https://doi.org/10.1002/adom.202002096>.

DOI: 10.1002/adom.202002096



Scheme 1. Subcomponent self-assembly of compounds **P-1**, **M-1**, **P-2**, **M-2**, **Δ-3**, and **Λ-3**.

MOCs.^[22–24] Here, the homochiral MOFs **P-1** and **M-1** could be synthesized from a 2:1:2 mixture of ZnBr_2 , 2,5-dimethyl-1H-imidazole-4-carboxaldehyde, 1R,2R-DCH or 1S,2S-DCH, in a mixed solvent of *N,N'*-diethylformamide and methanol (2:1, v/v) (for details, see the Supporting Information), respectively. By replacing 2,5-dimethyl-1H-imidazole-4-carboxaldehyde with 2-methyl-1H-imidazole-4-carboxaldehyde, homochiral MOFs **P-2** and **M-2** were obtained under the same conditions, while MOCs **Δ-3** and **Λ-3** were yielded by utilizing imidazole-4-carbaldehyde. These results indicate that the 2-methyl group on imidazole plays a structure-direct role on forming framework structures in **P-1**, **M-1**, **P-2**, and **M-2**. Similar phenomenon was observed in our previous report, in which the metal-organic tetartoidal cages were obtained with the 2-methyl group on the imidazolyl and cubic cages would be formed in the absence of steric effect of the 2-methyl group.^[25]

X-ray crystallography revealed that **P-1**, **P-2** crystallize in space group $P6_4$, while **M-1** and **M-2** crystallized in space group $P6_2$. The two enantiomeric pairs are isotopic (Figure S1a–d, Supporting Information). Hence the structural description is restricted to the **P-1**. The asymmetric unit of **P-1** contains one Zn^{II} ion, one Br anion, and a half of R-L1 ($R\text{-H}_2\text{L1} = N,N'\text{-}((1R,2R)\text{-cyclohexane-1,2-diyl})\text{bis}(1\text{-}(2,4\text{-dimethyl-1H-imidazol-5-yl})\text{methanimine})$). Each Zn^{II} ion adopts a tetrahedral geometry and coordinates with three nitrogen atoms ($\text{Zn-N } 1.993(4)\text{--}2.103(4) \text{ \AA}$) and one Br atom ($\text{Zn-Br } 2.3524(9) \text{ \AA}$, **Figure 1a**). In **P-1**, R-L1 is deprotonated and coordinated with four Zn^{II} ions, exhibits an “opened” conformation (Figure S2b, Supporting Information). The imidazolyl groups of R-L1 bridging Zn^{II} ions fabricate a trifold right-handed extensive helix in **P-1** with a pitch of 13.054 Å (Figure 1b). For **M-1**, the left-handed helix is formed by linking imidazolyl and Zn^{II} ions. The trifold helical chains are further linked by the cyclohexane groups to generate a 3D chiral porous framework, which contains 1D helical channels. The total potential solvent area volumes are

2956.1 Å³ (52.6%), 2884.4 Å³ (51.9%), 2823.2 Å³ (54.0%), and 2884.0 Å³ (55.7%) per unit cell for MOFs **P-1**, **M-1**, **P-2**, and **M-2**, respectively. By treating Zn^{II} as the vertices and both imidazolyl group and cyclohexane group of ligands as linkers, the frameworks can be simplified as chiral **eta** network (or (8,3)-a net, Figure S3, Supporting Information), which contains one kind of three-connected vertex and helices of one hand.^[26]

The enantiomers **Δ-3** and **Λ-3** crystallize in the chiral space group *R3*, which feature eight-nucleus chiral cubic cage structures (Figure 1d). The structure of **Δ-3** is described in detail. Two types of Zn^{II} centers are discovered in **Δ-3**. Six Zn^{II} ions adopt square-pyramidal coordination geometry (Figure 1c) and Zn^{II} center is chelated with one R-L3 ($R\text{-H}_2\text{L3} = N,N'\text{-}((1R,2R)\text{-cyclohexane-1,2-diyl})\text{bis}(1\text{-}(1H\text{-imidazol-5-yl})\text{methanimine})$) and bounded with one imidazole group from another R-L3 ($\text{Zn-N } 1.964(18)\text{--}2.177(12) \text{ \AA}$). Other two Zn^{II} ions adopt tetrahedral geometry and each Zn^{II} center is coordinated by three N atoms ($\text{Zn-N } 1.91(2)\text{--}2.028(10) \text{ \AA}$) and one Br anion ($\text{Zn-Br } 2.407(11)\text{--}2.410(7) \text{ \AA}$, Figure S1f, Supporting Information). Interestingly, the in situ formed R-L3 in **Δ-3** cages exhibit a “closed” conformation (Figure S2e,f, Supporting Information), which is obviously different from the “opened” conformation of the ligands in **P-1**, **P-2**, **M-1**, and **M-2**. The “closed” ligand link Zn^{2+} centers to form the chiral cubic cage structure of **Δ-3**.

The powder X-ray diffraction (PXRD) measurements of **P-1**, **M-1**, **P-2**, **M-2**, **Δ-3**, and **Λ-3** have shown that observed PXRD patterns are in good agreement with the simulated patterns (Figure S4, Supporting Information), suggesting pure phase of **P-1**, **M-1**, **P-2**, **M-2**, **Δ-3**, and **Λ-3** were successfully obtained. Thermogravimetric analysis and variable-temperature PXRD measurements revealed that **P-1**, **M-1**, **P-2**, **M-2**, **Δ-3**, and **Λ-3** are stable up to around 400 °C under N_2 atmosphere (Figure S5, Supporting Information) and around 250–350 °C in air (Figure S6, Supporting Information). We also checked the chemical

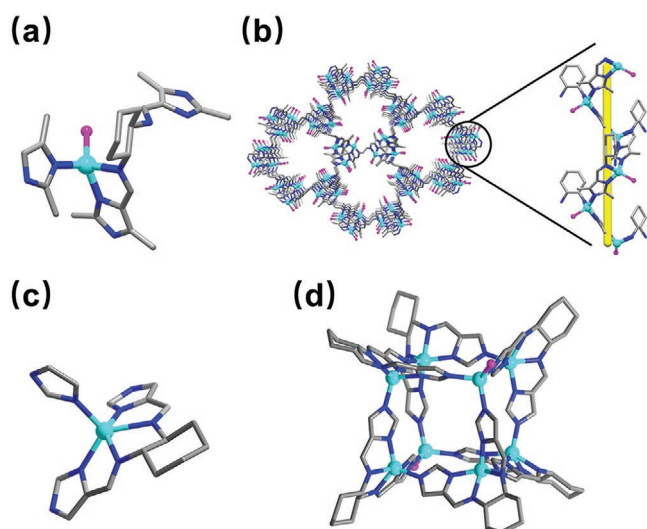


Figure 1. The single-crystal structures of **P-1**: a) coordination geometry of Zn^{II} and b) view of crystalline framework and the trifold right-handed helical chain. The single-crystal structures of Δ -3: c) the square-pyramidal coordination geometry of Zn^{II} center and d) view of chiral cubic cage structure. Color scheme: Zn, cyan; Br, pink; N, blue; C, gray; H, omitted.

stabilities of **P-1**, **P-2**, and Δ -3. The PXRD studies revealed that **P-1**, **P-2**, and Δ -3 are stable in common organic solvents (e.g., *N,N'*-dimethylformamide, MeOH, EtOH, and CH_3CN) and water at room temperature for 24 h (Figure S7, Supporting Information). N_2 gas adsorption measurements were performed at 77 K (Figures S8–S10, Supporting Information) for **P-1**, **M-1**, **P-2**, **M-2**, Δ -3, and Λ -3. Their Brunauer–Emmett–Teller surface areas were calculated to be 811, 843, 838, 833, 314, and 232 $m^2 g^{-1}$, respectively.

The photophysical properties of **P-1**, **M-1**, **P-2**, and **M-2** were first studied in solid-state. The solid-state UV–vis absorption spectra of **P-1** and **M-1** are identical (Figure 2a), showing main absorption peaks at around 313 nm, which can be ascribed to π – π^* transition of the imidazole rings. Similarly, both **P-2** and **M-2** show main absorption peaks at 310 nm (Figure S11a and Table S4, Supporting Information). The solid-state dichroism (CD) spectra have shown that **P-1** and **M-1** gave mirrored Cotton effect at 252 and 335 nm, respectively, which is in according with their opposite chirality (Figure 2b). The CD spectra of **P-2** and **M-2** are akin to **P-1** and **M-1** (Figure S11b, Supporting Information), respectively. For comparisons, the UV–vis and CD spectra of Δ -3 and Λ -3 were also performed in solid-state. The UV–vis spectra of Δ -3 and Λ -3 are identical and show a strong absorption maximum at around 286 nm (Figure S12a, Supporting Information). The CD spectra of Δ -3 and Λ -3 show the mirrored Cotton effect located on 246 and 323 nm (Figure S12b, Supporting Information), respectively, suggesting that Δ -3 and Λ -3 are chiral and a pair of enantiomers.

As shown in Figure 2c, the emission spectra of both **P-1** and **M-1** show a broad band centered at ≈ 520 nm at room temperature with a QY of 6.0% and 6.4%, which are comparable to other imidazolate-based framework, such as zeolitic imidazolate framework (ZIF)-8 (QY = 4.73%), ZIF-71 (QY = 9.13%), and ZIF-365 (5.21%).^[27–29] The average emission lifetime of **P-1** and **M-1** were 2.69 and 2.98 ns at 298 K (Table S4, Supporting Information), respectively. The short lifetime suggested they emitted fluorescence and the emission bands probably originated from intraligand charge-transfer. Notably, both **P-1** and **M-1** exhibited CPL response in the wavelength region of 450–650 nm (Figure 2d). The measured luminescence anisotropy factors (g_{lum} , defined as $g_{lum} = 2 \times (I_L - I_R)/(I_L + I_R)$, where I_L

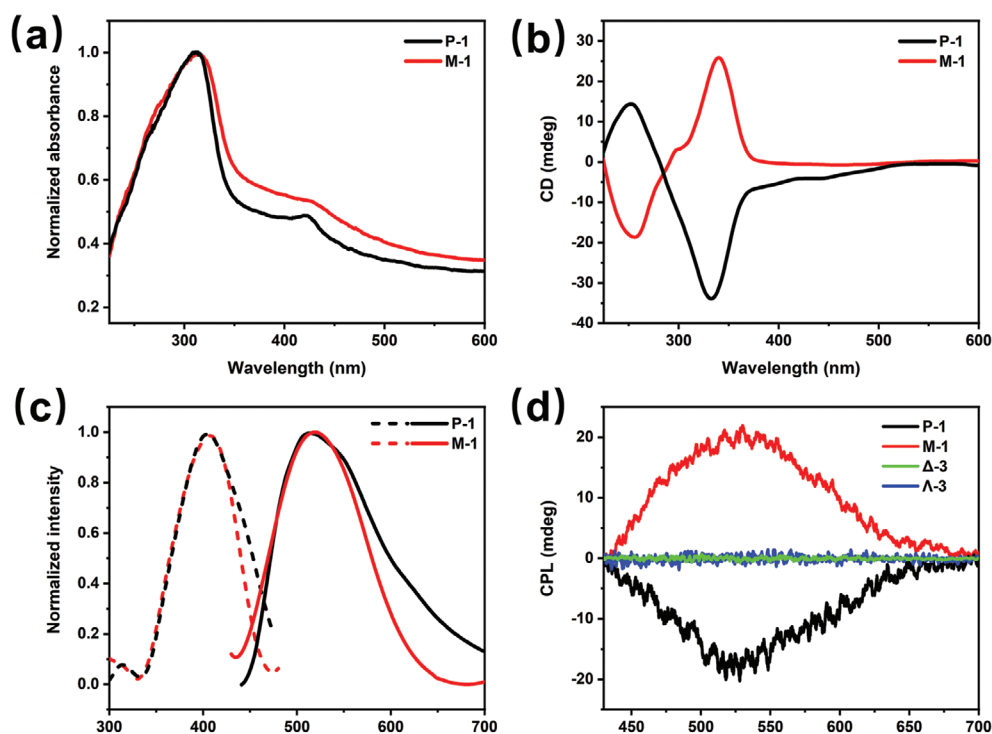


Figure 2. a) Normalized UV–vis absorption spectra, b) CD spectra, and c) normalized solid state excitation (dotted line) and emission spectra (solid line) of **M-1** and **P-1** in the solid state. d) CPL spectra of the **P-1** (red line), **M-1** (black line), Δ -3 (blue line), and Λ -3 (green line) in the solid state.

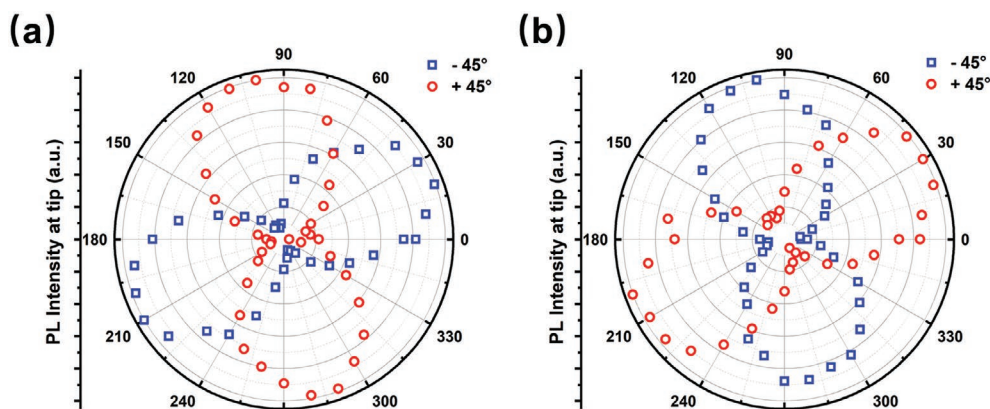


Figure 3. The PL intensity of a) the P-1 and b) M-1 as a function of the linear polarizer rotation angle, angle of $\lambda/4$ wave plate = $+45^\circ$ (red circles) and -45° (blue squares).

and I_R are the intensities of the left and right CPL, respectively) of P-1 and M-1 at 520 nm are about $\pm 2.3 \times 10^{-3}$, which are comparable to those of previously reported MOFs.^[11,12,14–18] For P-2 and M-2, both the PL/CPL properties are similar with that of P-1 and M-1 ($g_{lum} \approx 1.0 \times 10^{-3}$, Figure S13, Supporting Information). The Δ -3 and Λ -3 also displayed green emission (≈ 525 nm) with a QY of 6.0% and 5.5% at room temperature (Figure S12c, Supporting Information), respectively. Unexpectedly, both Δ -3 and Λ -3 are CPL silent (Figure 2d), although their PL properties and molecule structures of ligands are akin to that of P-1, M-1, P-2, and M-2. Thus, a CPL-on MOFs system is realized, which is probably due to the “opened” conformation of ligand and helical chain arrangement in the framework. In the literature, the

turn-on CPL of MOFs are usually realized by introducing chiral guests or luminophores into the cavities of the MOFs or chiral ligands on the surfaces of the MOFs.^[11,14–17,19] This is first time observation of turn-on CPL in MOFs by tuning the conformation of ligand.

To further check the CPL activity, the microarea CPL properties of single crystals of P-1 and M-1 were further measured by a homemade experimental setup (Figure S14a, Supporting Information).^[30,31] The continuous laser at 365 nm excited single crystals of P-1 and M-1, the emitted green light was detected by charge coupled device (CCD) detector (Figure S14b, Supporting Information). A quarter-wave plate ($\lambda/4$) was utilized to convert the circular polarization into a linear polarization state. The

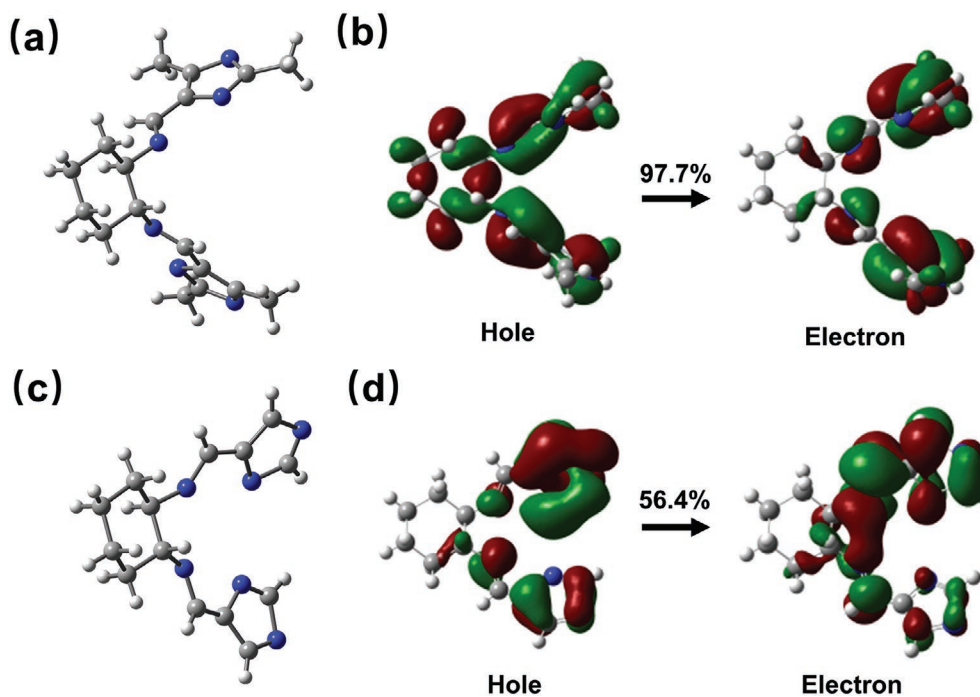


Figure 4. a) The “opened” conformation of R-L1 in P-1 and c) “closed” conformation of R-L3 in cage Δ -3. The calculated major NTOs responsible for the absorption b) at 360 nm of R-L1 and at d) 315 nm of R-3.

relationships between the maximum fluorescence intensity and rotating angle were recorded by fixing the fast axis of $\lambda/4$ wave plate and rotating the linear polarizer in front of a CCD with a step of 10° . As shown in **Figure 3a**, the maximum emission intensity values of a single-crystal **P-1** for -45° linear polarized light occurred at about 20° and 200° , while it occurred at about 110° and 290° for $+45^\circ$ linear polarized light, indicating the **P-1** is CPL-active. As expected, for **M-1**, the polarization directions of -45° linear polarized light and $+45^\circ$ linear polarized light are also nearly perpendicular (**Figure 3b**), which provide the solid evidence of CPL.

To understand the mechanism for turn-on CPL in MOFs, we subsequently performed DFT and time-dependent DFT calculations based on R-L1 and R-L3. The theoretical models of “opened” R-L1 and “closed” R-L3 were directly truncated from single-crystal structure of **P-1** and **Δ -3** (**Figure 4a,c**), respectively. The calculated major natural transition orbitals (NTOs) responsible for the absorption at 360 nm of R-L1 show that the charge transfer is from the chiral cyclohexane moiety to the imidazolyl luminophore (**Figure 4b**), while that of R-L3 shows more localized charge transfer character within imidazolyl groups (**Figure 4d**). The whole chiral cyclohexane group of R-L1 is involved in the charge transfer, which will probably yield the chiral excited electronic state to realize CPL activity. On the other hand, the imidazolyl groups bind with Zn^{II} to form extended trifold coordination helical chains in **P-1** (**Figure 2b**), which yield supramolecular chirality and will probably enhance the CPL activity of **P-1**.^[21] In contrast, oligomeric cubic cage structure in **Δ -3** (**Figure 2d**) will probably yield limited supramolecular chirality and not boost the CPL activity.

3. Conclusion

In summary, we have successfully synthesized and characterized a series of homochiral Zn-imidazolate 3D MOFs and cubic cages with similar CD spectra and PL properties. The formations of **eta** MOFs or cubic cages are regulated by the substituents, providing a clue to tune the structures of metal–organic assembles. Unusual photophysical properties have been observed: the MOFs feature CPL activity, while the luminescent chiral cages are CPL-silent. The turn-on CPL in MOFs by tuning the conformation of ligands and controlling the self-assembly will probably expand the possibilities of MOFs as CPL materials.

Supporting Information

Supporting Information is available from the Wiley Online Library or from the author.

Acknowledgements

This work was supported by the National Natural Science Foundation of China (Nos. 21731002, 21975104, and 21871172), the Guangdong Major Project of Basic and Applied Research (No. 2019B030302009), the Fundamental Research Funds for the Central Universities (No.

21619405), and Guangzhou Science and Technology Program (No. 202002030411). The computation in this work was supported by the high performance public computing service platform of Jinan University.

Conflict of Interest

The authors declare no conflict of interest.

Data Availability Statement

Research data are not shared.

Keywords

circularly polarized luminescence, metal–organic cages, metal–organic frameworks, self-assembly, supramolecular chirality

Received: December 5, 2020

Revised: December 24, 2020

Published online:

- [1] Y. Imai, Y. Nakano, T. Kawai, J. Yuasa, *Angew. Chem. Int. Ed.* **2018**, *57*, 8973.
- [2] R. Tempelaar, A. Stradomska, J. Knoester, F. C. Spano, *J. Phys. Chem. B* **2011**, *115*, 10592.
- [3] R. Carr, N. H. Evans, D. Parker, *Chem. Soc. Rev.* **2012**, *41*, 7673.
- [4] D.-Y. Kim, *J. Korean Phys. Soc.* **2006**, *49*, 505.
- [5] C. Wagenknecht, C.-M. Li, A. Reingruber, X.-H. Bao, A. Goebel, Y.-A. Chen, Q. Zhang, K. Chen, J.-W. Pan, *Nat. Photonics* **2010**, *4*, 549.
- [6] T. Islamoglu, Z. Chen, M. C. Wasson, C. T. Buru, K. O. Kirlikovali, U. Afrin, M. R. Mian, O. K. Farha, *Chem. Rev.* **2020**, *120*, 8130.
- [7] P.-L. Wang, L.-H. Xie, E. A. Joseph, J.-R. Li, X.-O. Su, H.-C. Zhou, *Chem. Rev.* **2019**, *119*, 10638.
- [8] H. C. Zhou, J. R. Long, O. M. Yaghi, *Chem. Rev.* **2012**, *112*, 673.
- [9] M. Yoon, R. Srirambalaji, K. Kim, *Chem. Rev.* **2012**, *112*, 1196.
- [10] Y. Liu, W. Xuan, Y. Cui, *Adv. Mater.* **2010**, *22*, 4112.
- [11] T. Zhao, J. Han, X. Jin, Y. Liu, M. Liu, P. Duan, *Angew. Chem., Int. Ed.* **2019**, *58*, 4978.
- [12] S. M. Chen, L. M. Chang, X. K. Yang, T. Luo, H. Xu, Z. G. Gu, J. Zhang, *ACS Appl. Mater. Interfaces* **2019**, *11*, 31421.
- [13] W. Shang, X. Zhu, T. Liang, C. Du, L. Hu, T. Li, M. Liu, *Angew. Chem., Int. Ed.* **2020**, *59*, 12811.
- [14] X.-H. Wu, Z. Wei, B.-J. Yan, R.-W. Huang, Y.-Y. Liu, K. Li, S.-Q. Zang, T. C. W. Mak, *CCS Chem.* **2019**, *1*, 553.
- [15] T. Zhao, J. Han, X. Jin, M. Zhou, Y. Liu, P. Duan, M. Liu, *Research* **2020**, *2020*, 6452123.
- [16] H. R. Fu, N. Wang, X. X. Wu, F. F. Li, Y. Zhao, L. F. Ma, M. Du, *Adv. Opt. Mater.* **2020**, *8*, 2000330.
- [17] C. Zhang, Z. P. Yan, X. Y. Dong, Z. Han, S. Li, T. Fu, Y. Y. Zhu, Y. X. Zheng, Y. Y. Niu, S. Q. Zang, *Adv. Mater.* **2020**, *32*, 2002914.
- [18] M. Zeng, A. Ren, W. Wu, Y. S. Zhao, C. Zhan, J. Yao, *Chem. Sci.* **2020**, *11*, 9154.
- [19] L. Hu, K. Li, W. Shang, X. Zhu, M. Liu, *Angew. Chem., Int. Ed.* **2020**, *59*, 4953.
- [20] Y. Sang, J. Han, T. Zhao, P. Duan, M. Liu, *Adv. Mater.* **2019**, *31*, 1900110.
- [21] J. Kumar, T. Nakashima, T. Kawai, *J. Phys. Chem. Lett.* **2015**, *6*, 3445.
- [22] Y. Wu, X. P. Zhou, J. R. Yang, D. Li, *Chem. Commun.* **2013**, *49*, 3413.
- [23] D. Luo, X. P. Zhou, D. Li, *Angew. Chem., Int. Ed.* **2015**, *54*, 6190.

- [24] X. P. Zhou, Y. Wu, D. Li, *J. Am. Chem. Soc.* **2013**, *135*, 16062.
- [25] D. Luo, X. Z. Wang, C. Yang, X. P. Zhou, D. Li, *J. Am. Chem. Soc.* **2018**, *140*, 118.
- [26] N. L. Rosi, J. Kim, M. Eddaoudi, B. Chen, M. O'Keeffe, O. M. Yaghi, *J. Am. Chem. Soc.* **2005**, *127*, 1504.
- [27] X. Yang, D. Yan, *Chem. Commun.* **2017**, *53*, 1801.
- [28] Y. Zhang, M. Gutierrez, A. K. Chaudhari, J. C. Tan, *ACS Appl. Mater. Interfaces* **2020**, *12*, 37477.
- [29] X. Z. Wang, Z. Q. Zhang, R. Guo, Y. Y. Zhang, N. J. Zhu, K. Wang, P. P. Sun, X. Y. Mao, J. J. Liu, J. Z. Huo, X. R. Wang, B. Ding, *Talanta* **2020**, *217*, 121010.
- [30] J. Peatross, M. Ware, *Physics of Light and Optics*, online textbook, available at optics.byu.edu, **2011**.
- [31] A. A. Kokhanovsky, *Light Scattering Reviews 4: Single Light Scattering and Radiative Transfer*, Springer Science & Business Media, Berlin **2009**.